6.7 A 1024×8 700ps Time-Gated SPAD Line Sensor for Laser Raman Spectroscopy and LIBS in Space and Rover-Based Planetary Exploration

Yuki Maruyama[1], Jordana Blacksberg[2], Edoardo Charbon[1]

[1]Delft University of Technology, Delft, The Netherlands,
[2]Jet Propulsion Laboratory, Pasadena, CA

Raman spectroscopy is a nondestructive, label-free optical analysis technique used to obtain structural and compositional information without any advance preparation. However, the Raman signature is often overwhelmed by strong fluorescence background. Due to its generation mechanism, the fluorescence background can be filtered out in the "time domain" even though it contains exactly the same wavelength components as the Raman signature. To realize such functionality, highly sensitive, time-resolved imagers, such as an intensified charge-coupled devices (iCCDs) or streak cameras are the sensors of choice. These delicate instruments are generally costly, bulky, and unsuitable for space flight and planetary landings. Time-gated, single-photon avalanche diode (SPAD) cameras have been studied for time-resolved imaging modalities, such as fluorescence lifetime imaging microscopy [1], taking advantage of SPAD picosecond temporal resolution as well as single-photon detection capability. Recently, a 128x128, time-gated SPAD array has been proposed to tackle fluorescence background reduction from highly fluorescent minerals for laser Raman spectroscopy targeting potential future on-surface planetary instruments [2]. However, due to long gating (~30ns), the obtained Raman signature was contaminated by background noise, which overcame minor Raman peaks. In addition, due to extensive on-pixel electronics, the fill factor was reduced, resulting in low photon detection efficiency (PDE). A larger SPAD with sub-nanosecond time-gating was proposed and implemented as a single pixel, operated with a mechanical scanning stage to obtain a Raman signature [3]. To avoid any mechanical moving parts or multiple detectors to obtain a complete Raman signature, a 2D array or line sensor format is thus required.

In this paper, we present an all-digital, 1024x8, time-resolved SPAD line sensor designed for time-resolved laser Raman spectroscopy and laser induced breakdown spectroscopy (LIBS). The block diagram of the system is shown in Fig. 6.7.1. The sensor consists of 16 groups of 64x8 SPAD arrays with fast readout interface electronics. The SPAD gate width and its delay are controlled by a combination of off-chip (Maxim DS1020, 1ns/tap) and on-chip delay lines (250ps/tap) resulting in a temporal resolution of 250ps through typical scan ranges of 32ns. Properly balanced binary trees allow less than 98.5ps skew variation across the entire chip. The proposed line sensor has a fill factor of 44.3% with a photon detection probability (PDP) of 21% at 475nm at an excess bias of 3.5V. The 24.6mm long focal plane matches the format of a typical detector that would be used at the output of a Raman spectrometer (e.g. CCD), allowing the observation of the entire Raman spectrum without the use of any moving parts, thus reducing complexity, overall power consumption, and weight.

The pixel schematic is shown in Fig. 6.7.2(a); it comprises a SPAD, implemented as shared cathode p+/deep n-well junction, a 1-bit counter, as well as a readout interface circuit. The pixel can be operated both in time-correlated single-photon counting (TCSPC) and time-uncorrelated photon counting (TUPC) modes. Time-resolved laser Raman spectroscopy and LIBS are achieved through signals 'spadoff' and 'recharge', with a subsequently applied 'gate' signal. These timing critical signals are propagated through binary trees and generated by carefully designed pulse generators (PG) in each row as shown in Fig. 6.7.2(b). Each pixel has an additional 1-bit memory, hot pixel elimination module (HPE), to locally turn off noisy pixels.

The chip, fabricated in a 0.35μm CMOS HV technology, has a total area of 29.64mm^2. The gating performance was first characterized in terms of its width and skew variations across the entire 24.7mm long chip. Figure 6.7.3(a) shows three examples of a gate of different widths verified optically, whereas the vertical axis represents time and the horizontal axis pixel position. The figure shows that the pixels are activated and deactivated with an accuracy better than 250ps and a negligible skew. Best gate width is chosen from 0.7ns to 12.6ns based on the photon return from the sample and the excitation laser pulse width. Figure 6.7.3(b) summarizes FWHM gate width variation for various gate widths. A 405nm pulsed laser source (Advanced Laser Diode Systems, Germany) with FWHM pulse width of 34ps was used to trigger an avalanche at the same time across the entire array. The optically measured minimum gate width is 0.7ns (σ = 120ps). While the SPAD is activated, the probability of detecting a dark count is decreased by the gate on/off ratio (as low as 5.3×10^{-4}%) at the minimum gate width of 0.7ns, whereby median dark count rate (DCR) of the device is 7.4kHz at an excess bias of 3.3V.

A 532nm (~20μJ/pulse, ~400ps pulse width, TEEM Photonics) laser, with ND filters to reduce the power on the sample, was used to create the Raman signature. The gating window shift with respect to the laser pulse allows us to obtain the Raman signature distribution in time with 250ps temporal resolution. Figure 6.7.4(a) shows the Raman signature obtained from Calcite with 3ns gating width in each delay line bin of 250ps. The output of 8 columns was summed in each row at each delay time. Figure 6.7.4(b) shows Raman peaks measured at a delay time of 16.75ns integrated over 10k frames. Preliminary results from mineral samples with strong fluorescence background (for example Willemite), were used to successfully confirm the background rejection capability of the gated SPAD sensor. The sensor was subsequently used to demonstrate its potential for use in planetary science as a combined Raman/LIBS instrument. Figure 6.7.5(a) shows an artist's rendering of the Curiosity rover analyzing the elemental composition of a rock on Mars using the laser-induced remote sensing instrument (ChemCam). The proposed SPAD line sensor is intended for use in a similar manner targeting not only LIBS but also time-resolved Raman spectroscopy [4]. Preliminary LIBS results show atomic lines from Barite at 75ns after the laser pulse as shown in Fig. 6.7.5(b). In the case of LIBS, as expected, laser-induced plasma appears prior to the atomic lines which can be used to determine elemental composition of rock and soil.

The Raman signature from highly fluorescent mineral samples was successfully observed, which was impossible to obtain in continuous wave (CW) Raman spectroscopy with 532nm excitation. These signals are in good agreement with the results taken by a streak camera, which requires high voltage and greater complexity with larger volume and weight. Figure 6.7.6(a) summarizes the performance of the chip, whereas Fig. 6.7.6(b) shows a comparison table with state-of-the-art sensors.

References:
[1] L. Pancheri, et al., "A SPAD-based Pixel Linear Array for High-Speed Time-Gated Fluorescence Lifetime Imaging", *European Solid-State Circuits Conf.*, pp. 428-431, Sep. 2009.
[2] J. Blacksberg, et al., "Fast single-photon avalanche diode arrays for laser Raman spectroscopy", *Optics letters*, vol. 36, pp. 3672-3674, Sep. 2011.
[3] I. Nissinen, et al., "A Sub-ns Time-gated CMOS Single Photon Avalanche Diode Detector for Raman Spectroscopy", *European Solid-State Device Research Conf.*, pp. 375-378, Sep. 2011.
[4] J. Blacksberg, et al., "Maximizing science return from a single on-surface mineralogy tool: combined Raman, LIBS, and fluorescence spectroscopy", *LPI Concepts and Approaches for Mars Exploration*, June 2012.
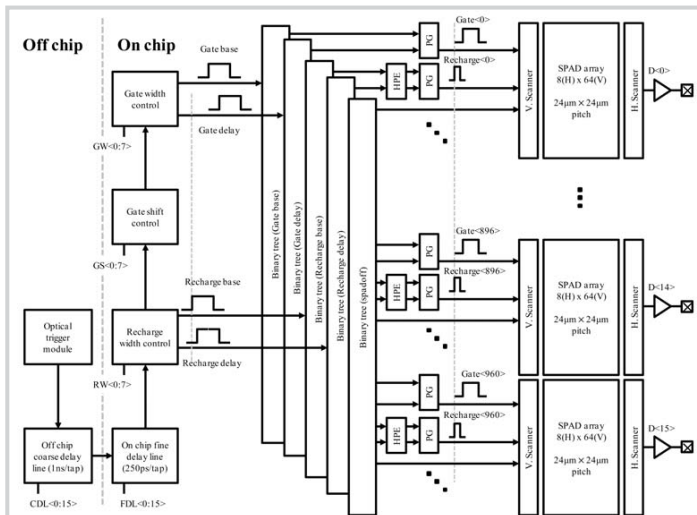
Figure 6.7.1: System block diagram showing pulse width control modules, off-chip and on-chip delay lines, hot pixel elimination modules (HPE), pulse generators (PG) and 16 groups of SPAD array.
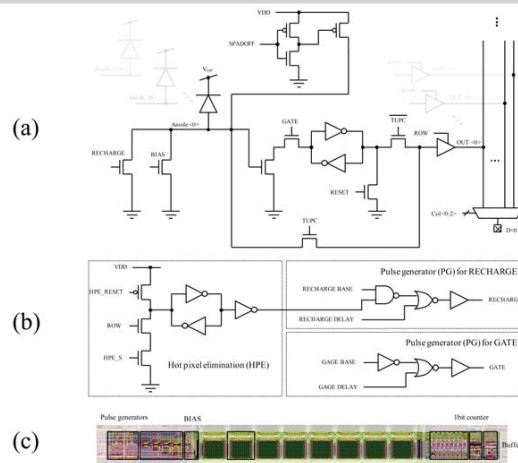
Figure 6.7.2: (a) Pixel schematic of the time-resolved SPAD line sensor. The pixel also has a bias transistor and a switch for the TUPC modality. (b) Hot pixel elimination module (HPE) and pulse generators (PG) for the RECHARGE and GATE signals. (c) Row level design of the chip.
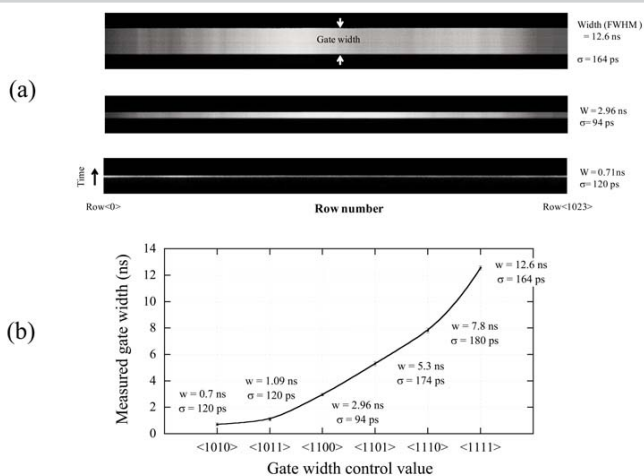
Figure 6.7.3: Summary of the gating mechanism measurements. (a) Raw output images at 12.6ns, 2.96ns and 0.71ns gate width. (b) Optically measured gate width across the 24.7mm long chip. FWHM gate width and its variations are measured over 200 frames.
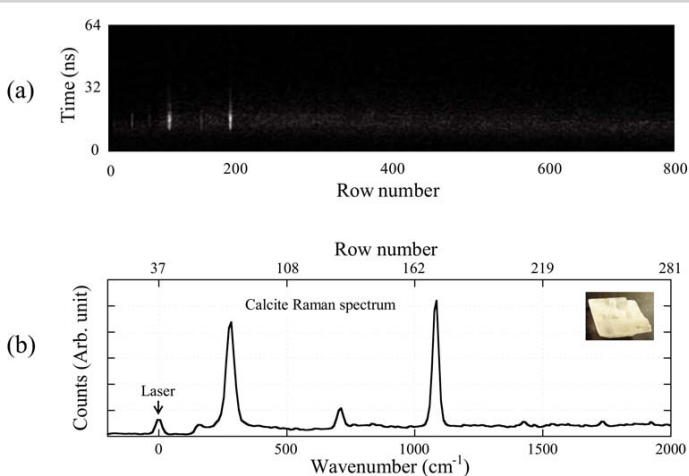
Figure 6.7.4: (a) Calcite Raman signature measured in time. (b) Raman peaks measured at delay time of 16.75ns. This spectrum was taken using a broad-band grating. With a standard Raman grating the Raman spectrum would be spread out over the entire chip with higher spectral resolution.
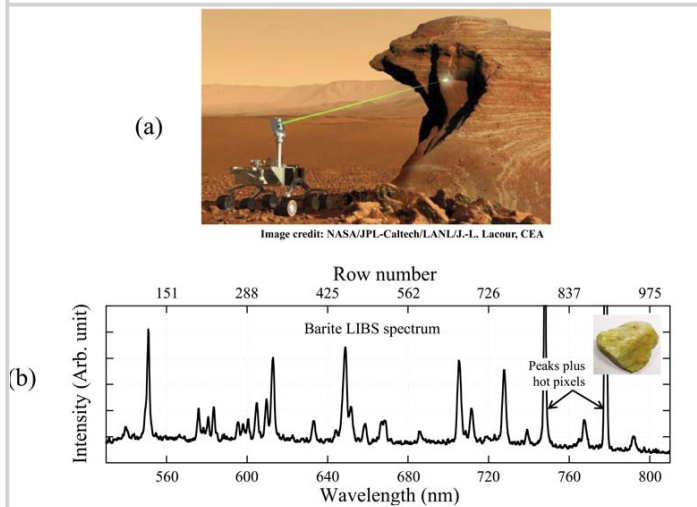
Figure 6.7.5: (a) Artist's rendering of the LIBS instrument (ChemCam) on the Curiosity rover. (b) LIBS spectrum from Barite at 75ns after the laser pulse. Note that this measurement is taken at a single gating time.

(a)

Performance measure	Min.	Typ.	Max.	Unit
Gate window (FWHM)	0.7 (σ = 120ps)		12.6 (σ = 164ps)	ns
Gate rise time		0.24 (jitter σ = 98.5ps)		ns
Gate fall time		1.00 (jitter σ = 93.6ps)		ns
Gating rep. rate	20		715	cycle/sec
Power dissipation		53		mW
Delay range	0 to 0.25	0 to 32	0 to 255	ns
Temporal resolution		250		ps
Delay line DNL (0 to 32ns)		68		ps
Delay line INL (0 to 32ns)		223		ps

(b)

Parameter	This work	Pancheri et al. [1]	Blacksberg et al. [2]	Nissinen et al. [3]	Unit
Technology	CMOS 0.35um HV	CMOS 0.35um HV	CMOS 0.35um HV	CMOS 0.35um HV	
Array format	1024 × 8	64 ×1	128 × 128	1	
Focal plane length	24,576	1,664	3,200	20	μm
SPAD active area per pixel	255.2	230	28.3 (6μm in diameter)	314 (20μm in diameter)	μm²
Detector pitch	24	26	25	N/A	μm
Fill factor	44.3	34	4.5	11	%
Photon detection probability	21 at λ = 475nm (Ve = 3.5V)	32 at λ = 450nm (Ve = 3.3V)	21 at λ = 475nm (Ve = 3.5V, w/o microlens)	N/A	%
Dark count rate (Ve = 3.3V)	7.4 (median)	1 (typ.)	0.16 (median)	11 (typ.)	kHz
Min. gate window	0.7	0.8	7	0.3	ns
Dark count probability per gating (Ve = 3.3V)	5.3 × 10⁻⁴	1.6 × 10⁻⁴	1.1 × 10⁻⁴	3.3 × 10⁻⁴	%
Application	Raman, LIBS and FLIM	FLIM	Raman	Raman	

Figure 6.7.6: (a) Performance summary of the imager and (b) comparison table. All measurements were conducted at room temperature.